THEORY-GUIDED SYNTHESIS OF AN ECO-FRIENDLY AND LOW-COST COPPER BASED SULFIDE THERMOELECTRIC MATERIAL

Kan Chen,[†] Baoli Du,[†] Nicola Bonini,[‡] Cedric Weber,[,‡] Haixue Yan,[†] and Mike J. Reece[†]*

[†]School of Engineering and Materials Science, Queen Mary, University of London, E1 4NS, UK

[‡]Department of Physics, King's College London, The Strand, WC2R 2LS, UK

*cedric.weber@kcl.ac.uk. +442078487165

Abstract

Cu_3SbS_4 is a copper-based sulfide composed of earth-abundant elements. We present a combined theoretical and experimental study of the thermoelectric properties of Ge-doped Cu_3SbS_4. Based on density functional theory, we found that the pristine compound is a semiconductor with a large density-of-state effective mass of ~ 2.2 m_e for holes. Ge was predicted to be an effective p-type dopant that only slightly shifts the band structure of Cu_3SbS_4. The power factor was predicted to reach a maximum value with 10 ~ 15 mol. % Ge-doping on the Sb site ($n = 6 \sim 9 \times 10^{20}$ cm^{-3}) at high temperature (up to 700 K). Theory was used to guide the synthesis of optimally doped Cu_3SbS_4 bulk samples. Experimentally, Cu_3SbS_4 bulk samples were prepared by mechanical alloying and spark plasma sintering. The samples had very fine microstructures, with grain size of ~ 100 to 300 nm, which contributed to a much lower lattice thermal conductivity than reported in the literature. A maximum power factor of ~ 1.08 $mWK^{-2}m^{-1}$ was achieved with an optimized carrier concentration of ~ 4.79×10^{20} cm^{-3}, which is in good agreement with theoretical prediction, and a zT of ~ 0.63 was obtained at 623 K.

Introduction

Thermoelectric (TE) technology, which can directly convert waste heat into useful electricity, is a potential solution to the global need for clean, safe and sustainable energy sources. The efficiency of TE devices is primarily determined by the material's dimensionless figure-of-merit, $zT = \alpha^2 T \rho^{-1} \kappa^{-1}$ where T is the absolute temperature, α is the Seebeck coefficient, ρ is the electrical resistivity, and κ is the thermal conductivity.[1] Several classes of thermoelectric materials are being investigated for renewable power generation applications including tellurides,[2] half-Heuslers,[3] and silicides.[4] Besides continuous efforts to improve the performance of traditional TE materials, there are many new TE materials being explored. Recent research has revealed that copper-based chalcogenides are promising TE materials, such as Cu(Ga, In)Te_2,[5-7] Cu_3SbSe_4,[8-9] $Cu_2ZnSnSe_4$,[10] Cu_2Se,[11-12] $Cu_{1.97}S$,[13] and $Cu_{12}Sb_4S_{13}$.[14-16] These copper-based chalcogenides show the common features of high Seebeck coefficients and intrinsically low thermal conductivities, which raised our interest in another copper-based chalcogenide, Cu_3SbS_4.

Cu_3SbS_4 is isostructural and isoelectronic to the good p-type thermoelectric material Cu_3SbSe_4 (zT value is above 0.8 at 650 K),[17] and it has the advantages of low-cost and low-toxicity. Cu_3SbS_4 crystallizes into an ordered zinc-blende superstructure with the space group $I\bar{4}2m$ (no.121) and lattice parameters of $a = 5.391(1)$ Å, $c = 10.764(1)$ Å.[18] As the lattice parameters match $c \approx 2a$ ($c/2a = 0.998$), the structure of Cu_3SbS_4 can be considered as a pesudocubic structure and it can realize cubic-like high degeneracy in its electronic bands, leading to a high thermopower.[7] Despite these features, little research has been done on the TE properties of Cu_3SbS_4. In the previous work, Cu_3SbS_4 samples were prepared by solid reaction combined with field assisted sintering. The samples had large grains of ~ 5 to 10 μm and

relatively high thermal conductivities of ~ 4 $Wm^{-1}K^{-1}$ at 300 K.[19-20] Pristine Cu_3SbS_4 showed a very high Seebeck coefficient of ~ 560 μVK^{-1}, but a high electrical resistivity of ~ 250 mΩcm. Both Ge and Sn have been used as dopants to improve the electrical properties of Cu_3SbS_4, leading to an enhanced power factor (PF), but the reported zT value was only 0.1 at 573 K.[19]

In this work, the Cu_3SbS_4 samples were prepared by mechanical alloying (MA) combined with sparking plasma sintering (SPS), which is an effective way to produce nano-structured materials. Ge was chosen as a p-type dopant on the Sb site to improve the electrical properties of Cu_3SbS_4 based on the previous research on Cu_3SbSe_4 and Cu_3SbS_4.[20-21] It has one less valence electron than Sb, similar ionic radius and preferred tetrahedral bonding like Sb. To guide the experimental work, theoretical predictions for the electronic structure, optimal doping concentration and thermoelectric properties of Ge-doped Cu_3SbS_4 were carried out based on density functional theory (DFT). The theory results indicate that Ge is an effective p-type dopant for Cu_3SbS_4 and the power factor (PF) can reach a maximum value with 10 ~ 15 mol. % Ge-doping on the Sb site at high temperature. The thermoelectric properties of the $Cu_3Sb_{1-x}Ge_xS_4$ (x = 0 ~ 0.15) samples were investigated from 300 K to 623 K, and showed good agreement with the theoretical results. The TE performance of Cu_3SbS_4 is significantly enhanced by Ge doping.

Theoretical and Experimental Methods

The theoretical studies were performed within DFT using the DFT+U approach (where we use the Perdew-Burke-Ernzerho exchange-correlation functional) as implemented in

the Quantum-Espresso code.[22-23] While standard DFT at the level of LDA or GGA predicts Cu_3SbS_4 to be a metallic compound, the DFT+U approach provides an effective way to recover the proper semiconductor band structure. As reported by Do et al.,[24] an unphysically large value of U (15 eV) for Cu can be used to obtain a band gap in reasonable agreement with experiments. However, this has a very large impact on the d-states of Cu, which are pushed to very low energies below the Fermi level because the Hartree energy of the Cu elements generates an unrealistic imbalance between the Cu and S energy levels. In this work we followed a strategy that is similar to the one used in the case of copper oxides, where it is crucial to also consider the Coulomb repulsion on the oxygen p-orbitals.[25] In particular, we found that a realistic Coulomb repulsion U for Cu (5 eV) and S (4 eV) results in a band gap which is in good agreement with experimental results.

In our calculations, we used the experimental structure (the theoretical prediction from DFT+U differs by less than 1% from the experimental data). The effect of Ge doping on the Sb site was modelled with a $2 \times 2 \times 2$ (64 atoms) supercell including structural relaxation (while keeping the experimental volume fixed). The formation energy was computed assuming the chemical potentials to be zero, which is appropriate for element-rich environments.[26] We used ultra-soft pseudopotentials with a cut-off on the wavefunction of 50 Ryd and a cut-off on the charge density of 400 Ryd. The sampling of the Brillouin zone was done with a $8 \times 8 \times 8$ ($4 \times 4 \times 4$) uniform mesh of k-points for unit cell ($2 \times 2 \times 2$ supercell) calculations. The electronic transport parameters (power factor and Seebeck coefficient) were computed using the Wannier interpolation with the BoltzWann code.[27] The temperature and doping level dependent transport properties were

computed using standard Boltzmann transport theory within the constant relaxation time approximation, and doping was simulated via a shift of the chemical potential. This approach has been shown to provide a good description of α(T) in a variety of thermoelectric materials.[27] We used a relaxation time of 2.22 ps, which lead to a good description of the electrical resistivities of the pristine and doped samples at high temperature.

Polycrystalline $Cu_3Sb_{1-x}Ge_xS_4$ samples with nominal doping of $x = 0$, 0.0125, 0.025, 0.05, 0.075, 0.1 and 0.15 were prepared by mechanical alloying (MA) combined with spark plasma sintering (SPS) (FCT, Rauenstein, Germany). Starting elements of Cu (99.5%, AlfaAesar), Sb (99.5%, AlfaAesar), Ge (99.999%, AlfaAesar), and S (reagent grade, purified by sublimation, Sigma-Aldrich) were ball milled in argon for 20 h. The obtained powders were loaded into a graphite die, and sintered using SPS at 723 K for 3 min at a pressure of 50 MPa.

The phases of the samples were examined using powder X-ray diffraction (XRD, Siemens D5000, CuKα). The microstructure was investigated using scanning electron microscopy (SEM, FEI, Inspect F, Hillsboro, OR) with energy dispersive X-ray spectroscopy (EDS). A bar of 3 mm $\times$ 3 mm $\times$ 15 mm was cut from the samples for electrical resistivity and Seebeck coefficient measurements using a ZEM-3 (ULVAC-RIKO) up to 623 K. The room temperature Hall coefficients were measured using the Van der Pauw method (The Lake Shore 8400 Series HMS). The thermal diffusivities were measured using the flash diffusivity method (LFA 457, Netzsch) up to 623 K. The specific heat capacities were calculated using the Dulong-Petit law. The densities were

measured using the Archimedes method. The thermal conductivities were calculated using the thermal diffusivity, specific heat capacity and density.

Results and Discussion

As a preliminary analysis to guide the synthesis of Ge-doped Cu_3SbS_4, we investigated from first-principles the electronic structure of the pristine compound and the effect of Ge- doping on the Sb site. Figure 1 shows the calculated band structure of pristine Cu_3SbS_4, and it has a band gap of ~ 0.6 eV, which is consistent with reported results.[28-29] A distinctive feature here is the presence of three distinct bands at the valence band maximum (VBM) at Γ, which results in a high density of states at the band edge. In particular, the density-of-state effective mass (m^*) of holes computed from DFT is 2.2 m_e (where m_e is the mass of the electron), which is larger than that reported for Cu_3SbSe_4 ($m^* = 1.1 \sim 1.7\ m_e$). This highlights the possibility to achieve a high Seebeck coefficient in p-type Cu_3SbS_4 sample.

To assess the effect of Ge-doping , we investigated the electronic structure of Cu_3SbS_4 with 12.5 mol. % Ge-doping on the Sb site. As shown in Figure 2, comparing with the density-of-state of pristine Cu_3SbS_4, the extra holes introduced by the Ge dopants slightly shifted the Fermi level, without altering the high density-of-state at the band edge of the pristine compound.

In order to predict the optimal doping level, the power factor for Ge-doped Cu_3SbS_4 as a function of Ge content was computed for different temperatures within the constant relaxation time approximation. As seen in Figure 3, the PF shows a maximum value when

the Ge content is about $x = 0.1 \sim 0.15$ at high temperature (below sintering temperature, 723 K).

Figure 4a shows the XRD results for $Cu_3Sb_{1-x}Ge_xS_4$ ($x = 0 \sim 0.15$). All of the samples appear to be phase pure, except the $x = 0.1$ and 0.15 samples for which an extra peak belonging to Cu_2GeS_3 is observed. From the enlarged figure, it can be seen that the peaks shift slightly to higher angles with increasing Ge content, which is a result of the fact that Ge has a slightly smaller ionic radius than that of Sb. The fractured surface of the undoped sample can be seen in Figure 4b. The sample has very fine grains ($100 \sim 300$ nm), which are much smaller than the grains ($3 \sim 10$ μm) of the sample prepared by solid state reaction.[20] This fine microstructure results from MA combined with SPS processing. The second phase was found in small amounts in all of the Ge-doped samples from SEM images. As shown in Figure 4c, the second phase is very distinct from the main phase; it has a much larger grain size (several micrometer). These observations indicate that the actual doping level is lower than the nominal Ge content because of the simultaneous formation of the Ge_2GeS_3 second phase.

To study the solubility and structural effects related to Ge doping, the formation energy of an $x = 0.125$ Ge doped sample was calculated. Without relaxing the structure, the calculated formation energy is -0.16 eV per Ge atom, showing that Ge is soluble. However, the formation energy improves significantly once the structure is relaxed, and the obtained formation energy is -0.68 eV. This clearly shows that there is a local restructuring around the Ge atoms (the distance between a Ge atom and the neighboring S atoms decreases by 6 % upon relaxation of the structure), which indicates that phase separation could be induced by Ge doping. In passing, it is interesting to note that the

formation energy of Ge defects obtained here is slightly lower than the value of -0.4 eV reported for Cu_3SbSe_4, and very similar to the formation energy of Sn defects in Cu_3SbSe_4 (-0.7 eV).[21]

Figure 5a shows the temperature dependence of the electrical resistivity. The electrical resistivity was significantly reduced by Ge doping over the investigated temperature range. The transport behavior changed from semiconductor for the undoped sample to metal-like for the doped samples. This confirms that Ge is an effective dopant to increase the carrier concentration. As seen in Table 1, all the samples have positive Hall coefficients indicating p-type conduction. The pristine Cu_3SbS_4 is an intrinsic semiconductor with a carrier concentration of around 10^{17} cm^{-3}. With Ge doping, the hole concentration increased up to 4.79×10^{20} cm^{-3} for the $x = 0.15$ sample. This is consistent with the measured electrical resistivity of the samples. In spite of the additional impurity phase, the $x = 0.15$ sample achieved a carrier concentration close to the predicted optimal concentration range. Figure 5b shows the temperature dependence of the Seebeck coefficient. The Seebeck coefficient decreased with increasing Ge doping, as the carrier concentration increased. The power factor was largely enhanced due to the optimized carrier concentration, which can be seen in Figure 5c.

Figure 6 shows a comparison of the theoretical results and experimental results. The carrier concentration dependence of theoretical and experimental Seebeck coefficient at 300 K is shown in Figure 6a. The experimental results are in good agreement with the theoretical results for all the samples, in spite of a small amount of second phase found in doped samples. It indicates the Ge-doping and the second phase produce no obvious disturbance of the band structure of Cu_3SbS_4 and the transport

properties are dominated by the main phase. The results were also examined by using a simple model based on a single parabolic band (SPB) with acoustic phonon scattering, which is often used for TE materials.[8, 30] The solid line represents the carrier concentration dependence of Seebeck coefficient based on the SPB model with a density-of-state effective mass (m^*) of 3.0 m_e, which is also known as Pisarenko line. All of the Ge-doped samples (with a small amount of second phase) are on the same Pisarenko line as the undoped sample (phase pure). It is important to note that the m^* estimated using the SPB model (3.0 m_e) is larger than that extracted from the DFT calculations (2.2 m_e). This suggests that effects beyond the single band approximation are important, but can be effectively simulated by an increased effective mass. However, both results reveal that Cu_3SbS_4 has a very large m^* among thermoelectric materials. A large m^* is favourable for high Seebeck coefficient. It can be used to explain the high Seebeck coefficient (670 μVK^{-1} at 300 K) in Cu_3SbS_4, which is higher than the value (375 μVK^{-1} at 300 K) reported in Cu_3SbSe_4 with an effective mass of about 1.5 m_e (estimated using the SPB model).[8]

In order to evaluate the results above 300 K, the carrier concentration was assumed to be constant with increasing temperature as the doped samples exhibited metal-like behavior. The temperature dependence of both theoretical and experimental Seebeck coefficient for the $x = 0.05$ sample is shown in Figure 6b. The experimental results show good agreement with theoretical results up to 623 K, which also applied to the other doped samples. Besides, the experimental power factors at 600 K are consistent with the theoretical predictions as shown in Figure 6c. The predicted maximum *PF* at

600 K was nearly achieved in the $x = 0.15$ sample with a carrier concentration of 4.79×10^{20} cm^{-3}.

The agreement between theory and experiment is excellent and provides a clear evidence of the very good quality of the electronic structure determined within GGA+U, and a validation of the theoretical approach used to model transport properties in Cu_3SbS_4 compound.

Figure 7 shows the temperature dependence of the total thermal conductivities and lattice thermal conductivities. For all of the samples, the thermal conductivity decreased with increasing temperature and there was no sign of bipolar effects. With Ge doping, the thermal conductivity increased over the investigated temperature range due to the increased electronic contribution. The insert figure shows the lattice thermal conductivity, which was calculated by subtracting the electronic thermal conductivity from the total thermal conductivity, $\kappa_L = \kappa - \kappa_e$. The electronic thermal conductivity was estimated based on the Wiedemann-Franz law, $\kappa_e = LT/\rho$, where L is the Lorenz number. L was calculated using the measured Seebeck coefficient based on the SPB model. The lattice thermal conductivity for pristine Cu_3SbS_4 is about 1.9 $Wm^{-1}K^{-1}$ at room temperature, which is much lower than the reported value of a sample prepared by solid reaction method.[20] The lower lattice thermal conductivity benefited from the MA and SPS processing, which produced a much smaller grain size ($100 \sim 300$ nm) than the solid reaction method ($3 \sim 10$ μm). The lattice thermal conductivities of all the samples decreased with a T^{-1} temperature dependence, indicating that phonon–phonon scattering (Umklapp process) was dominant for thermal transport over the investigated temperature range.[31]

Figure 8 shows the temperature dependence of the zT value for the $Cu_3Sb_{1-x}Ge_xS_4$ samples. As result of enhanced power factor and low thermal conductivity, a maximum zT value of 0.63 was achieved at 623 K in both $x = 0.1$ and 0.15 samples, which is the highest value reported in Cu_3SbS_4 compound so far.

Conclusions

This work shows that the eco-friendly and low-cost Cu_3SbS_4 compound is a promising thermoelectric material at medium temperature (around 623 K). In particular, our results show that Cu_3SbS_4 displays a high Seebeck coefficient that stems from the favourably high effective mass for holes. Ge is an effective p-dopant on the Sb site, which can introduce extra holes into the system with negligible effects on the electronic structure at the top of the valence band of Cu_3SbS_4. A relatively low thermal conductivity was achieved in nanostructured polycrystalline samples through a simple synthesis method of MA and SPS. These features result in a maximum figure of merit of 0.63 at 623 K with an optimized carrier concentration of $\sim 4.79 \times 10^{20}$ cm^{-3}. The excellent agreement between theory and experiment in a wide range of temperature and carrier concentration provides a clear evidence of the quality of the materials parameters (band structure, effective mass, defect formation energy) determined from first principles. The insight gained in this work into the doping and transport mechanisms in Cu_3SbS_4 will be essential for further optimization of this compound towards better TE performance. Finally, It would be interesting to extend the study to other similarly low-cost and copper-based sulfides, such as CuFeS2-type compounds, which also have large effective masses and power factors, but are however magnetic [32-33].

Acknowledgements

This work was supported by Engineering and Physical Sciences Research Council (EPSRC) (Grant no. EP/N0227261/1) and Designing Eco-Friendly and COst efficient Materials (DEFCOM). We thank Claire Burgess and Martyn A. McLachlan for helping with hall measurements. We thank Deepanshu Srivastava and Robert Freer for helping with Seebeck and resistivity measurements. K.C. acknowledges support from China Scholarship Council (CSC). B.D. acknowledges support from EU for individual Marie Curie Fellowship (Contract no. PIIF-GA-2013-622847). N.B. acknowledges support from EU FP7/CIG (Grant no. 294158). C.W. gratefully acknowledges the support of NVIDIA Corporation with the donation of the Tesla K40 GPUs used for this research. NB and CW acknowledge the ARCHER UK National Supercomputing Service.

References

(1) Rowe, D. M., *Crc Handbook of Thermoelectrics*; CRC Press, 1995.

(2) Gelbstein, Y.; Dashevsky, Z.; Dariel, M. P., In-Doped $Pb_{0.5}Sn_{0.5}Te$ P-Type Samples Prepared by Powder Metallurgical Processing for Thermoelectric Applications. *Phys. B* **2007**, *396*, 16-21.

(3) Kirievsky, K.; Shlimovich, M.; Fuks, D.; Gelbstein, Y., An Ab Initio Study of the Thermoelectric Enhancement Potential in Nano-Grained TiNiSn. *Phys. Chem. Chem. Phys.* **2014**, *16*, 20023-20029.

(4) Sadia, Y.; Dinnerman, L.; Gelbstein, Y., Mechanical Alloying and Spark Plasma Sintering of Higher Manganese Silicides for Thermoelectric Applications. *J. Electron. Mater.* **2013**, *42*, 1926-1931.

(5) Zhang, J.; Qin, X. Y.; Li, D.; Xin, H. X.; Song, C. J.; Li, L. L.; Zhu, X. G.; Wang, Z. M.; Guo, G. L.; Wang, L., Enhanced Thermoelectric Performance of $CuGaTe_2$ Based Composites Incorporated with Nanophase Cu_2Se. *J. Mater. Chem. A* **2014**, *2*, 2891-2895.

(6) Plirdpring, T., et al., Chalcopyrite $CuGaTe_2$: A High-Efficiency Bulk Thermoelectric Material. *Adv. Mater.* **2012**, *24*, 3622-3626.

(7) Zhang, J. W.; Liu, R. H.; Cheng, N. A.; Zhang, Y. B.; Yang, J. H.; Uher, C.; Shi, X.; Chen, L. D.; Zhang, W. Q., High-Performance Pseudocubic Thermoelectric Materials from Non-Cubic Chalcopyrite Compounds. *Adv. Mater.* **2014**, *26*, 3848-3853.

(8) Wei, T. R.; Wang, H.; Gibbs, Z. M.; Wu, C. F.; Snyder, G. J.; Li, J. F., Thermoelectric Properties of Sn-Doped P-Type Cu_3SbSe_4: A Compound with Large Effective Mass and Small Band Gap. *J. Mater. Chem. A* **2014**, *2*, 13527-13533.

(9) Yang, C.; Huang, F.; Wu, L.; Xu, K., New Stannite-Like P-Type Thermoelectric Material Cu_3SbSe_4. *J. Phys. D: Appl. Phys.* **2011**, *44*, 295404.

(10) Shi, X. Y.; Huang, F. Q.; Liu, M. L.; Chen, L. D., Thermoelectric Properties of Tetrahedrally Bonded Wide-Gap Stannite Compounds $Cu_2ZnSn_{1-x}In_xSe_4$. *Appl. Phys. Lett.* **2009**, *94*,122103.

(11) Su, X., et al., Self-Propagating High-Temperature Synthesis for Compound Thermoelectrics and New Criterion for Combustion Processing. *Nat. Commun.* **2014**, *5*.

(12) Liu, H. L., et al., Ultrahigh Thermoelectric Performance by Electron and Phonon Critical Scattering in $Cu_2Se_{1-x}I_x$. *Adv. Mater.* **2013**, *25*, 6607-6612.

(13) He, Y.; Day, T.; Zhang, T.; Liu, H.; Shi, X.; Chen, L.; Snyder, G. J., High Thermoelectric Performance in Non-Toxic Earth-Abundant Copper Sulfide. *Adv. Mater.* **2014**, *26*, 3974-3978.

(14) Heo, J.; Laurita, G.; Muir, S.; Subramanian, M. A.; Keszler, D. A., Enhanced Thermoelectric Performance of Synthetic Tetrahedrites. *Chem. Mater.* **2014**, *26*, 2047-2051.

(15) Lu, X.; Morelli, D. T.; Xia, Y.; Ozolins, V., Increasing the Thermoelectric Figure of Merit of Tetrahedrites by Co-Doping with Nickel and Zinc. *Chem. Mater.* **2015**, *27*, 408-413.

(16) Chetty, R.; Bali, A.; Mallik, R. C., Tetrahedrites as Thermoelectric Materials: An Overview. *J. Mater. Chem. C* **2015**, *3*, 12364-12378.

(17) Skoug, E. J.; Cain, J. D.; Morelli, D. T., High Thermoelectric Figure of Merit in the Cu_3SbSe_4-Cu_3SbS_4 Solid Solution. *Appl. Phys. Lett.* **2011**, *98*, 261911.

(18) Pfitzner, A. R., S., Refinement of the Crystal Structures of Cu_3PS_4 and Cu_3SbS_4 and a Comment on Normal Tetrahedral Structures. *Z. Kristallogr.* **2002**, *217*, 51-54.

(19) Yosuke Goto, Y. S., Yoichi Kamihara, Masanori Matoba, Effect of Sn-Substitution on Thermoelectric Properties of Copper-Based Sulfide, Famatinite Cu_3SbS_4. *J. Phys. Soc. Jpn.* **2015**, *84*, 044706.

(20) Suzumura, A.; Watanabe, M.; Nagasako, N.; Asahi, R., Improvement in Thermoelectric Properties of Se-Free Cu_3SbS_4 Compound. *J. Electron. Mater.* **2014**, *43*, 2356-2361.

(21) Do, D. T.; Mahanti, S. D., Theoretical Study of Defects in Cu_3SbSe_4 Search for Optimum Dopants for Enhancing Thermoelectric Properties. *J. Alloy. Compd.* **2015**, *625*, 346-354.

(22) Perdew, J. P.; Burke, K.; Ernzerhof, M., Generalized Gradient Approximation Made Simple. *Phys. Rev. Lett.* **1996**, *77*, 3865-3868.

(23) Giannozzi, P., et al., Quantum Espresso: A Modular and Open-Source Software Project for Quantum Simulations of Materials. *J. Phys. Condens. Matter.* **2009**, *21*, 395502.

(24) Do, D. T.; Mahanti, S. D., Bonds, Bands, and Band Gaps in Tetrahedrally Bonded Ternary Compounds: The Role of Group V Lone Pairs. *J. Phys. Chem. Solids* **2014**, *75*, 477-485.

(25) Hybertsen, M. S.; Schlüter, M.; Christensen, N. E., Calculation of Coulomb-Interaction Parameters for La_2cuo_4 Using a Constrained-Density-Functional Approach. *Phys. Rev. B* **1989**, *39*, 9028-9041.

(26) Zhang, S. B.; Northrup, J. E., Chemical Potential Dependence of Defect Formation Energies in GaAs: Application to Ga Self-Diffusion. *Phys. Rev. Lett.* **1991**, *67*, 2339-2342.

(27) Pizzi, G.; Volja, D.; Kozinsky, B.; Fornari, M.; Marzari, N., Boltzwann: A Code for the Evaluation of Thermoelectric and Electronic Transport Properties with a Maximally-Localized Wannier Functions Basis. *Comput. Phys. Commun.* **2014**, *185*, 422-429.

(28) Du, J.; Yu, Z.; Zhang, J., Preparation of Cu_3SbS_4 Thin Films with LBL Method. *Electronic Components & Materials* **2005**, *4*, 24-27.

(29) Skoug, E. J.; Cain, J. D.; Morelli, D. T.; Kirkham, M.; Majsztrik, P.; Lara-Curzio, E., Lattice Thermal Conductivity of the Cu_3SbSe_4-Cu_3SbS_4 Solid Solution. *J. Appl. Phys.* **2011**, *110*, 023501.

(30) Ioffe, A. F. *Semiconductor Thermoelements, and Thermoelectric Cooling*; Infosearch, ltd., London, 1957.

(31) Toberer, E. S.; Zevalkink, A.; Snyder, G. J., Phonon Engineering through Crystal Chemistry. *J. Mater. Chem.* **2011**, *21*, 15843-15852.

(32) Tsujii, N.; Mori, T., High Thermoelectric Power Factor in a Carrier-Doped Magnetic Semiconductor $CuFeS_2$. *Appl. Phys. Express* **2013**, *6*, 043001.

(33) Ang, R.; Khan, A. U.; Tsujii, N.; Takai, K.; Nakamura, R.; Mori, T., Thermoelectricity Generation and Electron–Magnon Scattering in a Natural Chalcopyrite Mineral from a Deep-Sea Hydrothermal Vent. *Angew. Chem. Int. Edit.* **2015**, *54*, 12909-12913.

Tables

Table 1. Room temperature Hall coefficient, carrier concentration, carrier mobility, Seebeck coefficient and electrical resistivity of $Cu_3Sb_{1-x}Ge_xS_4$ ($x = 0 \sim 0.15$) samples.

Nominal doping	Hall coefficient R_H (cm^3C^{-1})	Carrier concentration n ($10^{20}cm^{-3}$)	Carrier mobility μ ($cm^2V^{-1}s^{-1}$)	Seebeck coefficient α (μVK^{-1})	Electrical resistivity ρ ($\mu\Omega m$)
$x = 0$	19	0.0032	16.46	670.1	11231.9
$x = 0.0125$	0.45	0.13	9.33	351.7	625.3
$x = 0.025$	0.19	0.33	6.82	284.5	196.3
$x = 0.05$	0.064	0.98	5.28	208.7	107.5
$x = 0.075$	0.039	1.61	5.32	174.2	49.1

$x = 0.10$	0.020	3.07	5.22	150.8	35.7
$x = 0.15$	0.013	4.79	5.33	113.7	19.4

Figure Captions

Figure 1. Band structure of Cu_3SbS_4 with the GGA+U method (left) and corresponding density-of-state (right).

Figure 2. Total density-of-state of pristine Cu_3SbS_4 and 12.5 mol. % Ge-doped Cu_3SbS_4. The DOS of the pristine compound (dashed line) has been shifted to account for the extra hole introduced by Ge-doping.

Figure 3. Theoretical power factor (PF) as a function of nominal Ge content (x) at 500, 600 and 700 K.

Figure 4. (a) XRD patterns of $Cu_3Sb_{1-x}Ge_xS_4$ ($x = 0 \sim 0.15$) samples after SPS, (b) SEM image of fracture surface of Cu_3SbS_4 and (c) SEM image of fracture surface of $Cu_3Sb_{1-x}Ge_xS_4$ ($x = 0.0125$) showing the second phase.

Figure 5. The temperature dependence of (a) electrical resistivity (ρ), (b) Seebeck coefficient (α) and (c) power factor (PF) for $Cu_3Sb_{1-x}Ge_xS_4$ ($x = 0 \sim 0.15$) samples.

Figure 6. (a) The theoretical and experimental Seebeck coefficient (α) as a function of carrier concentration (n) at 300 K and the Pisarenko line with $m^* = 3.0\ m_e$, (b) the temperature dependence of theoretical and experimental Seebeck coefficient (α) for $x = 0.05$ sample, and (c) the theoretical and experimental power factor (PF) as a function of carrier concentration (n) at 600 K.

Figure 7. The temperature dependence of thermal conductivity (κ) and lattice thermal conductivity (κ_L) (insert) for $Cu_3Sb_{1-x}Ge_xS_4$ ($x = 0 \sim 0.15$) samples.

Figure 8. The temperature dependence of zT value for $Cu_3Sb_{1-x}Ge_xS_4$ ($x = 0 \sim 0.15$) samples.

Figure 1

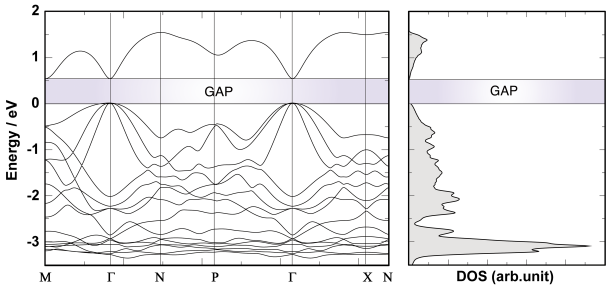

Figure 2

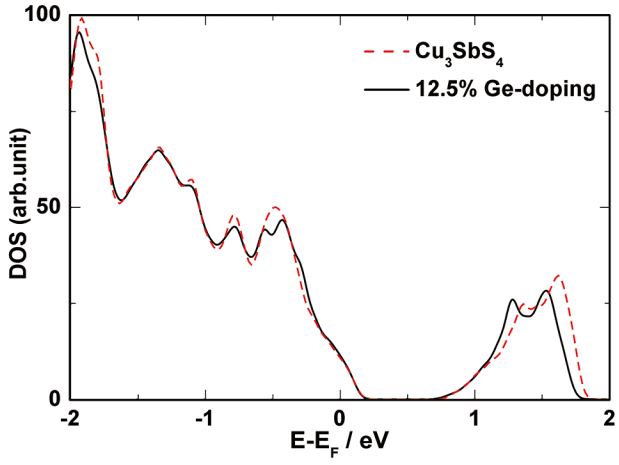

Figure 3

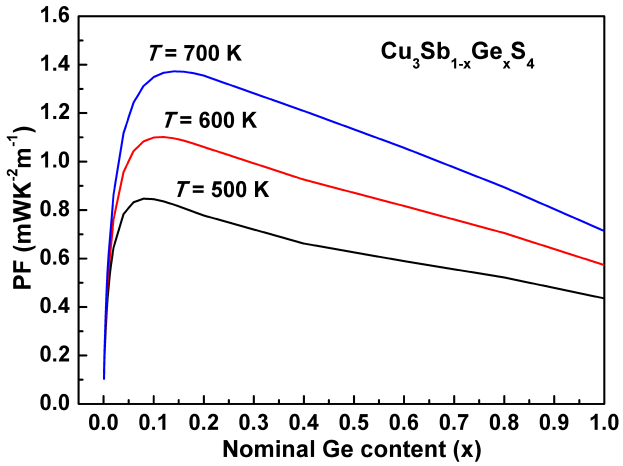

Figure 4

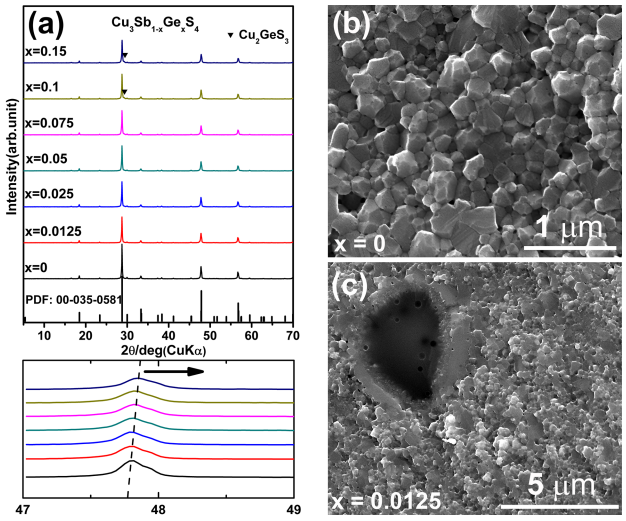
(a)
Cu3Sb1-xGexS4
Cu2GeS3
x=0.15
x=0.1
x=0.075
x=0.05
x=0.025
x=0.0125
x=0
PDF: 00-035-0581
Intensity(arb.unit)
10
20
30
40
50
60
70
2θ/deg(CuKα)
47
48
49
(b)
x = 0
1 μm
(c)
x = 0.0125
5 μm

Figure 5

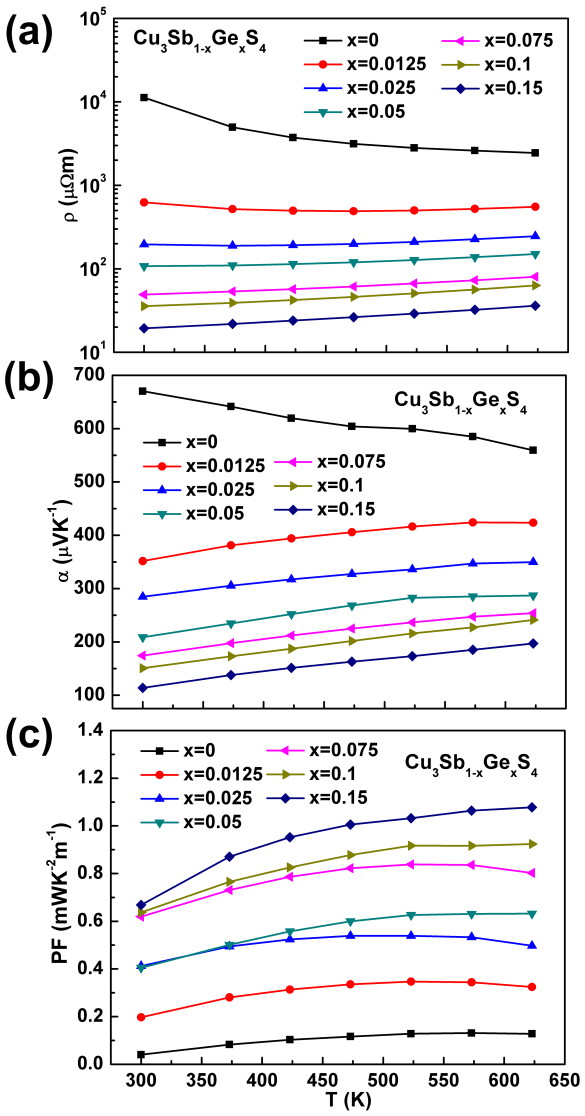
(a)
Cu3Sb1-xGexS4
x=0
x=0.0125
x=0.025
x=0.05
x=0.075
x=0.1
x=0.15
ρ (μΩm)
(b)
α (μVK-1)
(c)
PF (mWK-2m-1)
T (K)

Figure 6

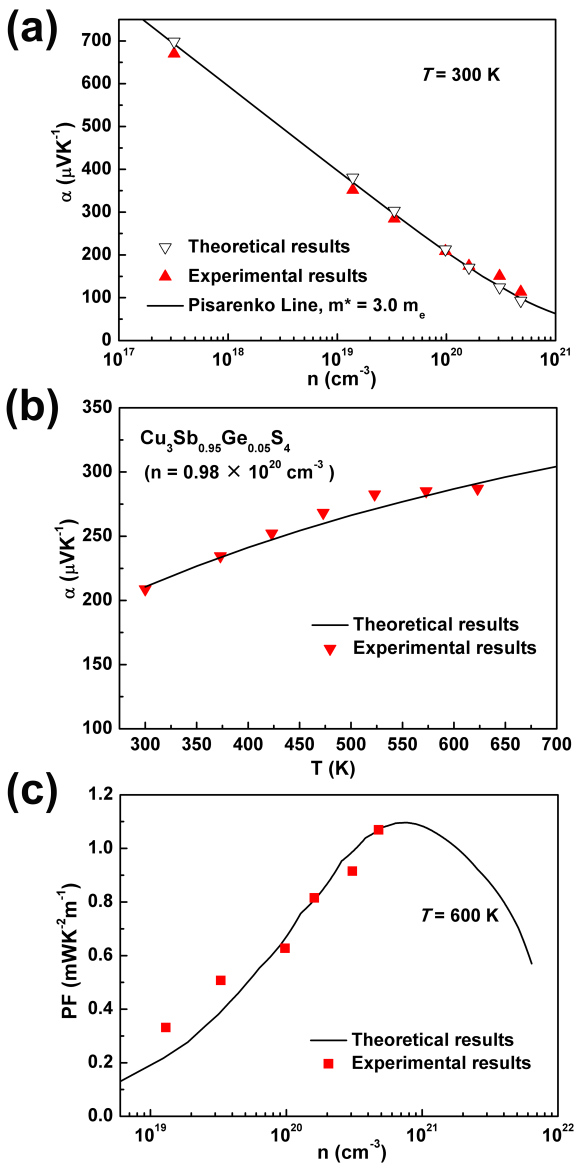
(a)
T = 300 K
α (μVK-1)
Theoretical results
Experimental results
Pisarenko Line, m* = 3.0 me
n (cm-3)
(b)
Cu3Sb0.95Ge0.05S4
(n = 0.98 × 10^20 cm-3)
α (μVK-1)
Theoretical results
Experimental results
T (K)
(c)
T = 600 K
PF (mWK-2m-1)
Theoretical results
Experimental results
n (cm-3)

Figure 7

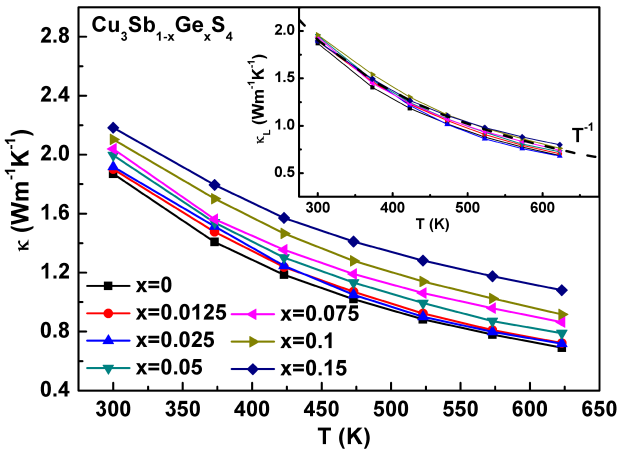

Figure 8

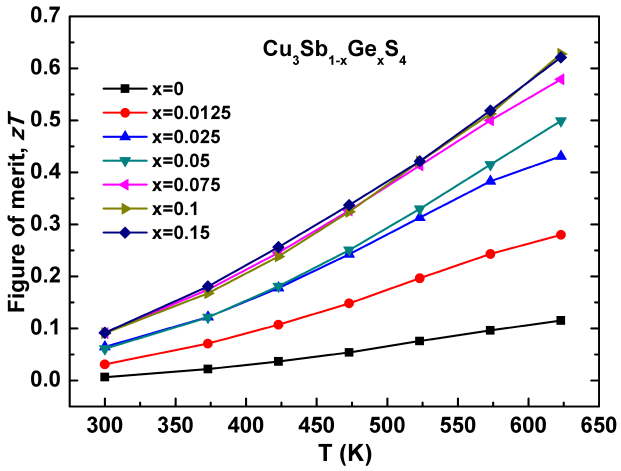

Table of Contents (TOC) Image

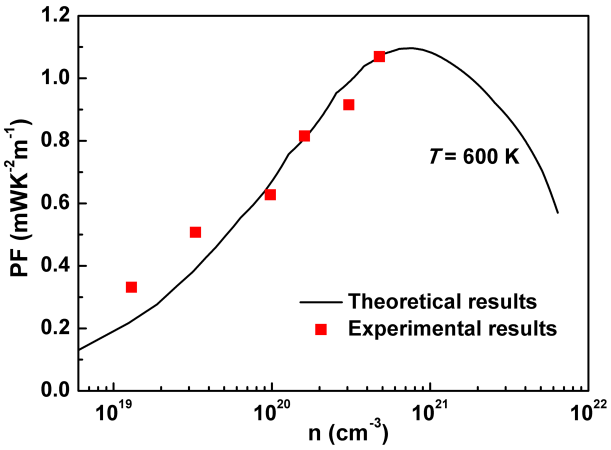
1.2
1.0
0.8
0.6
0.4
0.2
0.0
PF (mWK-2m-1)
T = 600 K
Theoretical results
Experimental results
10^19
10^20
10^21
10^22
n (cm-3)